Nonlinear interactions between high-Q optical and acoustic modes in dielectric particles

G. Gantzounis,[1,*] N. Papanikolaou,[1] and N. Stefanou[2]
[1]*Institute of Microelectronics, NCSR "Demokritos," GR-153 10 Athens, Greece*
[2]*University of Athens, Section of Solid State Physics, Panepistimioupolis, GR-157 84 Athens, Greece*
(Received 14 July 2011; published 29 September 2011)

The interaction between acoustic breathing modes and optical Mie resonances in a spherical particle made of a chalcogenide glass material is investigated by means of rigorous calculations, correct to any order in the acousto-optic coupling parameter. Our results reveal the occurrence of strong effects beyond the linear-response approximation, which lead to enhanced modulation of light by acoustic waves through multiphonon exchange mechanisms when both photons and phonons have a very long lifetime inside the particle.

DOI: 10.1103/PhysRevB.84.104303 PACS number(s): 78.20.hb, 46.40.−f, 43.40.+s, 63.20.Pw

I. INTRODUCTION

The vision of compact miniaturized optical components and cirquits has fueled active, intensive research on the modulation and control of light. Several proposals based on two-photon absorption of free carriers in semiconductors,[1,2] or nonlinear materials where the refractive properties can be controled electro-optically or thermo-optically[3,4] have been reported. On the other hand, carefully engineered optical modes like waveguide, slow-light, or cavity modes are often used to achieve enhanced nonlinear phenomena.[5–9]

Light modulation by acoustic phonons through the so-called acousto-optic (AO) interaction has been used for several decades now in optical systems. Acoustic waves with frequencies in the MHz range are usually generated by piezoelectric transducers, while much higher frequencies can also be achieved through heating by a femtosecond pulsed laser.[10] An acoustic wave causes a modulation of the material optical response in two ways: through the motion of the interfaces (interface effect) and through the change of the refractive index (bulk effect). In the interior of a homogeneous material, only the bulk AO effect, which depends on the corresponding AO coefficients that describe the influence of the local stress field on the refractive properties, is appropriate. On the contrary, in nanostructured materials with large surface areas like slot waveguides and slabs, the interface contribution alone seems to explain the observed effects and has been exploited to achieve efficient coupling of mechanical oscillations with light. This proved very fruitful leading to applications such as cooling of mechanical oscillators toward the quantum regime[11] and optomechanically induced transparency,[9] with impact in both fundamental and applied physics. In the general case, however, both interface and bulk AO effects need to be considered.

Light modulation was used to study acoustic phonons, from GHz up to THz frequencies, in periodic multilayer structures through pump-probe techniques,[12–14] while the effect of cavity resonances, either optical or both optical and acoustic, in such structures has also been considered.[5] Strong AO interaction can result from simultaneous localization of the elastic and electromagnetic (EM) fields and careful design of their overlap.[15] Therefore dual phononic-photonic cavities were fabricated by semiconductor multilayers to explore the influence of the simultaneous localization of the fields in the same region of space on the AO interaction.[12,16,17] In a recent study of the AO interaction in a Si/SiO_2 multilayer structure, it was suggested that simultaneous localization of photons and phonons in a resonant cavity could trigger multiphonon absorption processes.[18] Similarly, generation of cascaded vibrational modes was reported through optically induced mechanical vibrations of a simultaneously optical and acoustic wispering-galery-mode (WGM) resonator.[19] Stimulated Brillouin scattering could be enhanced by increasing the AO interaction but, due to the requirement of frequency and momentum matching,[3] it is hard to be detected in cavities and WGM resonators.[20] On the other hand, strong optomechanical coupling was also demostrated on slab waveguides and nanobeams for telecom frequencies and sound from MHz up to GHz frequencies.[21,22]

In this paper, we investigate spherical dielectric particles that exhibit simultaneously optical and acoustic resonances as potential candidates to enhance the AO interaction and achieve strong modulation of light through excitation of their acoustic eigenmodes. More specifically, we consider a spherical particle made of a chalcogenide glass material, subjected to excitation of its acoustic breathing modes by a femtosecond visible light pulse, and monitor the modulation of the optical scattering cross section over a broad wavelength range in the near-infrared region. Our work is motivated by recent experimental studies of the elastic properties of homogeneous[23,24] and coated[25,26] metallic nanoparticles in a dielectric matrix. A similar technique to probe changes in the reflectivity under a femtosecond laser pumping was also reported for layers of Au-capped polystyrene spheres.[27,28] It is worth noting that in contrast to recent studies of optomechanical coupling in WGM resonators, where the optical modulation is accounted for by changes in the resonator shape,[19,29] in the present work, we consider a system where the interface effect is less important and the occurring phenomena are mainly due to the bulk AO effect.

II. OPTICAL EXCITATION OF ACOUSTIC MODES

We consider a spherical particle with radius $R = 500$ nm, made of the amorphous chalcogenide glass a-As_2S_3, in air. The fabrication of such spherical chalcogenide glass spheres of varying diameter coupled to a Si waveguide was recently demonstrated.[30] The specific glass material was chosen because it is characterized by two AO coefficients which are almost equal to each other. This implies an isotropic change in the refractive index of the strained material, which greatly

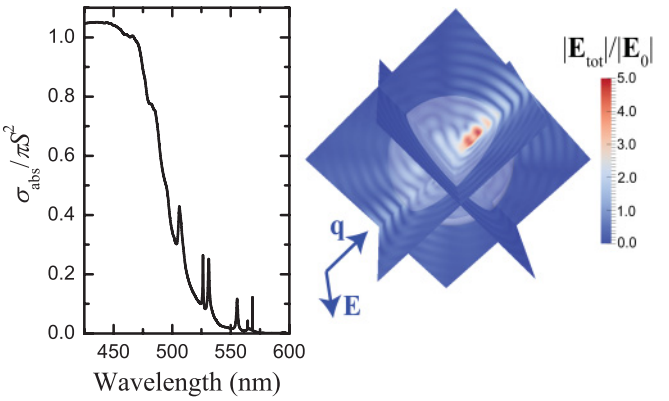

FIG. 1. (Color online) A spherical particle of radius 500 nm made of a-As_2S_3: optical absorption cross section spectrum (left) and total electric field distribution upon illumination at a wavelength of 500 nm (right).

facilitates the theoretical description. Moreover, the high refractive index of a-As_2S_3 also helps to obtain an enhanced bulk AO effect.

In Fig. 1, we display the optical absorption spectrum of the particle under consideration in the optical region, calculated using the experimental refractive index of a-As_2S_3,[31] which decreases smoothly from about 2.8 at 500 nm to about 2.5 at 1050 nm. It can be seen that below 550 nm, there is a progressive increase in the absorption cross section, because of the corresponding increase of the imaginary part of the dielectric function. The distinct peaks in the absorption spectrum are related to the absorption of Mie resonant modes. Therefore, if we illuminate the particle with a laser beam below ~550 nm, a considerable amount of energy will be absorbed and transferred to phonons. As shown in Fig. 1, at these wavelengths, the EM field penetrates throughout the particle and is more or less homogeneously distributed. It is then plausible to assume that ultrafast heating of the particle by a femtosecond laser beam induces a homogeneous thermal stress and triggers radial mechanical vibrations about the new equilibrium position. The corresponding displacement field has the form $\mathbf{U}(\mathbf{r},t) = U(r,t)\hat{\mathbf{r}}$, where $U(r,t)$ satisfies the equation of motion

$$\frac{1}{c_l^2}\frac{\partial^2 U(r,t)}{\partial t^2} = \frac{\partial^2 U(r,t)}{\partial r^2} + \frac{2}{r}\frac{\partial U(r,t)}{\partial r} - 2\frac{U(r,t)}{r^2}\,, \qquad (1)$$

and the associated stress dyadic takes the form $\boldsymbol{\sigma}(\mathbf{r},t) = \sigma_{rr}(r,t)\hat{\mathbf{r}}\hat{\mathbf{r}}$, where

$$\sigma_{rr}(r,t) = \rho c_l^2\left[\frac{\partial U(r,t)}{\partial r} + 2\left(1 - 2\frac{c_t^2}{c_l^2}\right)\frac{U(r,t)}{r}\right], \qquad (2)$$

with the mass density $\rho = 3.08$ gr/cm^3, and the longitudinal and transverse sound velocities $c_l = 2685$ m/s and $c_t = 1436$ m/s, respectively, of a-As_2S_3. We are searching for time-harmonic solutions of Eq. (1), in the form

$$U(r,t) = \Re\mathrm{e}[u(r)\exp(-i\Omega t)]\,. \qquad (3)$$

The time-independent equation satisfied by $u(r)$ constitutes for a free particle, a Sturm-Liouville problem with boundary conditions $u(r=0) = 0$, $\sigma_{rr}(R) = 0$, and

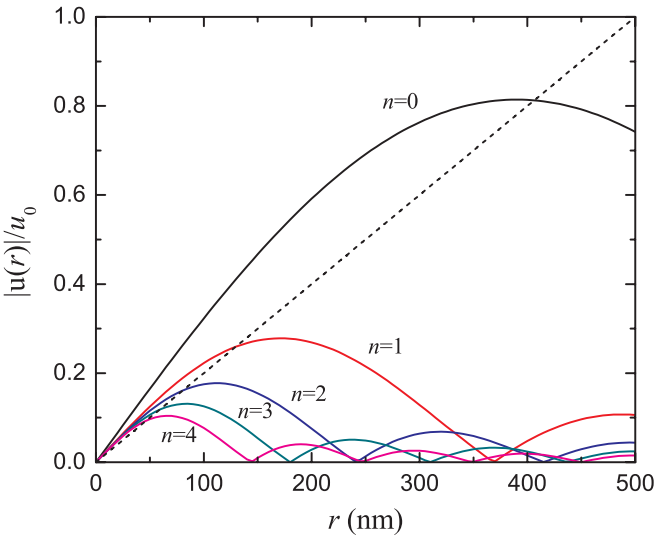

FIG. 2. (Color online) Projection of the initial displacement field (broken line) onto the first five acoustic breathing modes ($n = 0$–4) of the spherical particle under consideration.

weight function $w(r) = r^2$. The corresponding eigenfunctions $u_n(r) = j_1(\Omega_n r/c_l)$, $n = 0,1,\ldots$, with the spherical Bessel function of first kind and order one j_1[32] and the corresponding angular eigenfrequencies Ω_n, form an orthonormal basis set of acoustic breathing modes, which can be used for the expansion of any radial displacement field.

When the particle is embedded in air ($\rho = 0.00123$ gr/cm^3, $c_l = 340$ m/s, $c_t = 0$), the eigenfrequencies Ω_n become complex due to leakage of the acoustic field in air. Of more importance are the dissipative losses in the particle, which become dominant in the GHz region. These losses can be taken into account assuming frequency-dependent complex velocities: $(1 - i\alpha f)c_l$ and $(1 - i\alpha f)c_t$ for the longitudinal and transverse elastic waves in the particle, respectively, with $f = \Omega/2\pi$ and a typical value of $\alpha = 10^{-4}$ GHz^{-1}.[33]

The initial radial displacement field is a time-independent solution of Eq. (1) that vanishes at the origin and thus takes the form $-u_0 r/R$, where u_0 is the appropriate amplitude and the minus sign denotes initial compression from the equilibrium state.[34] Due to this initial displacement the particle will start to vibrate and the corresponding radial displacement field can be written in the form

$$\mathbf{U}(r,t) = \Re\mathrm{e}\left[\sum_n c_n u_n(r)\exp(-i\Omega_n t)\right]\hat{\mathbf{r}}\,, \qquad (4)$$

with the expansion coefficients c_n evaluated by projecting the initial displacement field onto the acoustic breathing modes of the particle. The projection of the initial displacement field onto the first five ($n = 0$–4) acoustic breathing modes is shown in Fig. 2. The eigenfrequencies f_n and corresponding lifetimes τ_n of these modes are given in Table I.

III. ACOUSTO-OPTIC EFFECTS

The spherical geometry of the problem under study greatly simplifies the analysis of the AO interaction. The strain field

TABLE I. Eigenfrequencies and corresponding lifetimes of the first five acoustic breathing modes of the spherical particle under consideration.

n	f_n (GHz)	τ_n (ns)
0	2.282	273
1	5.206	58
2	7.949	25
3	10.661	14
4	13.362	9

associated with a spherically symmetric acoustic displacement field, described by Eq. (4), takes the form

$$S_{ab}(\mathbf{r},t) \equiv \frac{1}{2}\left[\frac{\partial U_a}{\partial x_b} + \frac{\partial U_b}{\partial x_a}\right] = \left[\frac{\partial U(r,t)}{\partial r} - \frac{U(r,t)}{r}\right]\frac{x_a x_b}{r^2} + \frac{U(r,t)}{r}\delta_{ab}, \quad (5)$$

where $a,b = 1,2,3$ denote cartesian components. This strain field induces a change in the dielectric tensor $\delta\bar{\epsilon}$ of the material which, for small strains, i.e. in the linear regime, is given by

$$[\delta\bar{\epsilon}^{-1}]_{ab} \equiv [\bar{\epsilon}^{-1}]_{ab} - [\bar{\epsilon}_r^{-1}]_{ab} = \sum_{cd} p_{abcd} S_{cd}, \quad (6)$$

where $\bar{\epsilon}$ and $\bar{\epsilon}_r$ are the dielectric tensors of the strained and unstrained (reference) material, respectively, and p_{abcd} are the Pockels elasto-optic coefficients.[35] For an amorphous material, e.g., a polycrystalline or amorphous solid, $p_{2222} = p_{3333} = p_{1111} \equiv p_{11}$ and $p_{1133} = p_{2211} = p_{2233} = p_{3311} = p_{3322} = p_{1122} \equiv p_{12}$, i.e., there are just two independent Pockels coefficients. In the particular case of a-As_2S_3 $p_{12} \cong p_{11}$ (=0.25),[36] which implies an isotropic change in the refractive index of the strained material given by

$$\Delta n(r,t) = -\frac{1}{2} n_r^3 p_{11}\left[\frac{\partial U(r,t)}{\partial r} + 2\frac{U(r,t)}{r}\right], \quad (7)$$

where n_r is the refractive index of the unstrained a-As_2S_3. We note that in our calculations the maximum strain level never exceeds 1%, which is below the material limit. Besides the change in the refractive index, the strain field induces a change in the size of the particle. In order to accurately describe these two effects in the given spherical particle, we divide it into N shells. The ith shell has an external radius R_i and an average refractive index n_i (=n_r for the unperturbed particle). Under the influence of an acoustic field, these quantities vary in time as follows

$$R_i(t) = R_i + U(R_i,t) \quad (8)$$

and

$$n_i(t) = n_r + \Delta n\left(\frac{R_i + R_{i-1}}{2}, t\right). \quad (9)$$

IV. INELASTIC LIGHT SCATTERING

The time variation of the EM field in the presence of an acoustic field can be described in the quasistatic approximation. Let us consider the variation of the optical scattering cross section. We assume a plane monochromatic EM wave, of angular frequency ω and wavevector $\mathbf{q}$ in air, of the form $\mathbf{E}(\mathbf{r},t) = \Re\mathrm{e}[\mathbf{E}_0 \exp[i(\mathbf{q}\cdot\mathbf{r} - \omega t)]$, incident on the given particle. Such a plane wave can be expanded into regular vector spherical waves,[37] with appropriate multipole coefficients a^0_{Plm}, where $P = E$ or H denotes electric or magnetic polarization, respectively, and $l = 1,2,\ldots, m = -l,\ldots,l$ are the usual angular momentum indices. Correspondingly, the scattered field can be expanded into outgoing vector spherical waves. The expansion coefficients of the scattered field, a^+_{Plm}, are given in terms of a^0_{Plm} through the corresponding T matrix, which is diagonal in Plm and independent of m ($T_{Plm;P'l'm'} = T_{Pl}\delta_{PP'}\delta_{ll'}\delta_{mm'}$) because of the spherical symmetry of the scatterer: $a^+_{Plm} = T_{Pl}a^0_{Plm}$. For multishell spheres, the scattering T matrix can be calculated numerically using an efficient recursive procedure.[38] The optical scattering cross section, defined as the total power scattered by the particle per unit incident flux averaged over a period of the EM wave, is given by

$$\sigma^0_{\mathrm{sc}} = \frac{1}{q^2|\mathbf{E}_0|^2}\sum_{Plm}|a^+_{Plm}|^2 = \frac{\pi}{q^2}\sum_{Pl}(2l+1)|T_{Pl}|^2. \quad (10)$$

In the presence of the AO interaction, the refractive index varies very slowly compared to the period of the EM wave [see Eq. (7)], since $\omega/2\pi \approx 300$ THz. Therefore, we can describe the scattered field by introducing multipole coefficients, $a^+_{Plm}(t)$, which exhibit an accordingly slow time variation and thus can be assumed to be constant over a period of the EM wave (quasi-static approximation), leading to a time-dependent scattering cross section

$$\sigma_{\mathrm{sc}}(t) = \frac{1}{q^2|\mathbf{E}_0|^2}\sum_{Plm}|a^+_{Plm}(t)|^2\,. \quad (11)$$

To begin with, we assume excitation of the fundamental ($n = 0$) breathing mode only and neglect losses, since the lifetime of the mode is very long compared to its time period. In this case, the vibration of the particle is periodic, with a frequency f_0 (see Table I). Therefore, the multipole coefficients of the scattered field also oscillate periodically in time with the same frequency f_0 and thus can be expanded into a Fourier series

$$a^+_{Plm}(t) = \sum_{n=0,\pm1,\pm2,\ldots}\tilde{a}^+_{Plm}(n)\exp(-i2\pi n f_0 t)\,. \quad (12)$$

The optical response of the particle under consideration exhibits in the near-infrared region a number of transverse electric (TE) and transverse magnetic (TM) Mie resonances,[39] as shown in the upper diagram of Fig. 3. For reasons explained above, the acoustic wave field induces a quasi-stationary perturbation in the optical response of the particle through the AO effect [Eqs. (8) and (9)] and, as a result, the whole optical scattering spectrum oscillates in time, with more or less the same amplitude (wavelength or frequency variation, see the insets of Fig. 3). Subdividing the particle into $N = 40$ shells we accurately describe these effects with a relative error less than 10^{-4}. In the lower panel of Fig. 3, we show in more detail the change in the frequency $\Delta\omega$ of two specific Mie resonances: TE_7 with a high quality factor $Q = 1480$ at 769 nm and TM_4 with a low quality factor $Q = 21$ at 1021 nm. Strong photon-phonon interaction is expected if both light and sound

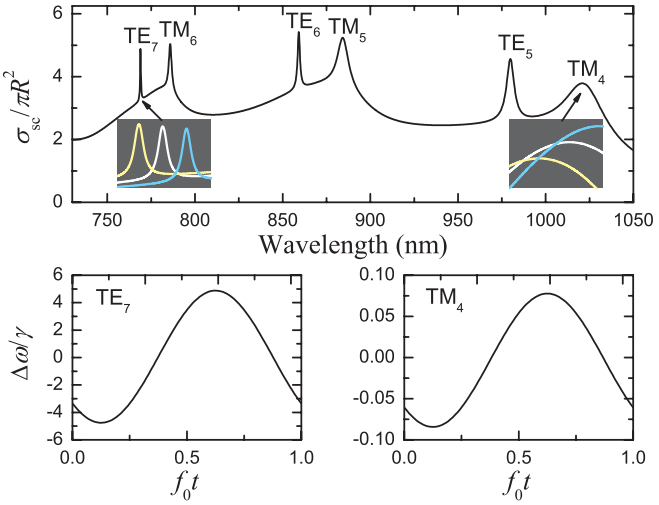

FIG. 3. (Color online) Upper diagram: the optical scattering cross section of the particle under consideration, in the near-infrared region. The insets display the variation of the TE_7 and TM_4 Mie resonances, in a window of 5 nm, upon excitation of the fundamental acoustic breathing mode of the particle at a level corresponding to $u_0 = 0.1$ nm (the curves on both sides of each resonance of the unperturbed particle correspond to snapshots at which maximum shift is obtained). Lower diagrams: oscillation of the TE_7 and TM_4 Mie resonances as a function of time (note the different scales in the ordinates).

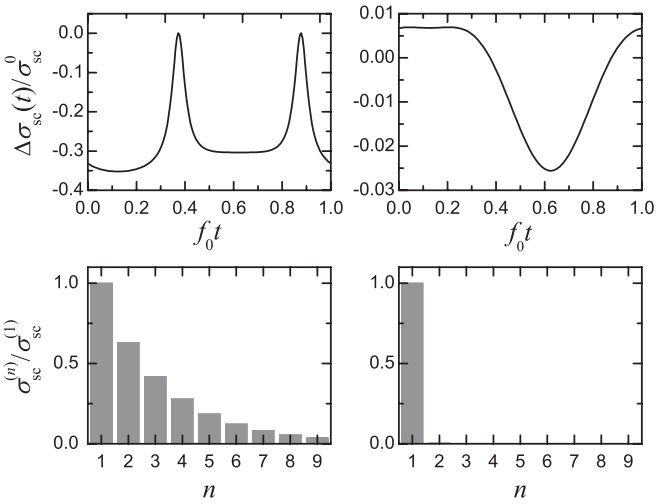

FIG. 4. Optical scattering cross section of the particle under consideration for the high-Q TE_7 mode (left-hand panel) and for the low-Q TM_4 mode (right-hand panel), upon excitation of its acoustic breathing mode at a level corresponding to $u_0 = 0.1$ nm. Time variation of the perturbed scattering cross section [upper diagrams, Eq. (11)] and partial cross sections associated with the Fourier components of the scattered field [lower diagrams, Eq. (13)].

have long lifetimes in the particle. The maximum frequency variation of a Mie resonance is proportional to the acoustic field intensity in the particle, i.e., the number and the lifetime of phonons. However, in order to compare the variation of the two Mie resonances, it is appropriate to consider the frequency shifts multiplied by the respective photon lifetimes $\tau \propto 1/\gamma$. Large-amplitude oscillations of $\Delta\omega/\gamma$ in the bottom diagrams of Fig. 3 are related to simultaneous localization of photons and phonons for a long time in the particle, which leads to strong AO interaction. As discussed above, one can clearly identify two distinct contributions in the AO interaction: the change in the particle radius and the change in the refractive index of the material. The calculations show that, in our case, the latter is about 95% of the whole effect for both the high-Q TE_7 and the low-Q TM_4 optical modes and, therefore, inelastic light scattering (ILS) is mainly due to the bulk AO interaction. The percentage of the bulk AO contribution depends on the shape of the optical and acoustic modes involved. Low-order Mie resonances and acoustic breathing modes overlap strongly within the whole volume of the particle and, for particles with large AO coefficients, give rise to a pronounced bulk AO effect. For a micrometric As_2S_3 particle, low-order Mie resonances appear in the near-infrared region. In contrast, higher-order optical modes are localized close to the particle surface. This is similar to WGM resonators and optomechanical coupling observed in particles with diameters of hundreds of microns, where the size variations appear to provide the dominant contribution.[19,29] Shrinking the particle size down to the micron scale shifts WGM to short wavelengths, where absorption dominates. Using materials that combine high refractive index with strong AO coefficients allows for enhanced AO effects even in submicron particles.

The AO interaction causes a temporal variation of the optical properties, measured directly by pump-probe time-resolved techniques and consequent ILS measured by Brillouin or Raman experiments. The change in the scattering cross section, $\Delta\sigma_{sc}(t) \equiv \sigma_{sc}(t) - \sigma_{sc}^0$, induced by the AO effect in the high-Q TE_7 mode and the low-Q TM_4 mode is displayed in the upper diagrams of Fig. 4. In the case of strong AO interaction, which leads to large-amplitude oscillations of $\Delta\omega/\gamma$ (bottom left diagram of Fig. 3), there are abrupt changes of the scattering cross section with time, as shown in the top left diagram of Fig. 4. On the contrary, if the AO interaction is relatively weak and the oscillations of $\Delta\omega/\gamma$ have a small amplitude, the scattering cross section shows a slow variation with time, as depicted in the top right diagram of Fig. 4. To determine the ILS spectrum, we consider the average scattering cross section $\langle\sigma_{sc}\rangle$ calculated over a period of the acoustic wave

$$\langle\sigma_{sc}\rangle = \frac{f}{q^2|\mathbf{E}_0|^2}\sum_{Plm}\int_0^{1/f} dt\,|a^+_{Plm}(t)|^2$$
$$= \sum_n \frac{1}{q^2|\mathbf{E}_0|^2}\sum_{Plm}|\tilde{a}^+_{Plm}(n)|^2 \equiv \sum_n \sigma_{sc}^{(n)}\,, \quad (13)$$

where $\sigma_{sc}^{(n)}$ corresponds to the scattering cross section associated with the nth ILS process, which involves absorption or emission of n phonons by the photon. We note that $\sigma_{sc}^{(n)} = \sigma_{sc}^{(-n)}$, for given n; this is why in the lower diagrams of Fig. 4, we show the relative intensity of $\sigma_{sc}^{(n)}$ for $n > 0$. When strong ILS takes place, the scattering process is not linear in the AO coupling parameter and many terms are needed in the expansion of the scattered field which, in the particle picture, implies strong probability amplitudes for multiphonon absorption and emission processes (see bottom left diagram of Fig. 4). On the other hand, when either the phonons or the photons have not long enough lifetimes, the corresponding Fourier spectrum is essentially dominated by

the first-order terms (see bottom right diagram of Fig. 4), which is the behavior expected in a usual pump-probe or Brillouin/Raman scattering experiment where single-phonon processes are involved and expansion up to first order in Eq. (12) is sufficient (Stokes and anti-Stokes components). The partial scattering cross sections shown in the lower diagrams of Fig. 4 in the frequency domain are appropriate to an ILS experiment. We note that these are not obtained through a Fourier transform of the time-dependent scattering cross sections shown in the upper diagrams of Fig. 4, which are appropriate to a time resolved experiment. Recently, the excitation of cascaded vibrational modes was measured, and multiple Stokes lines and third harmonic generation were reported in optomechanically coupled WGM resonators.[19] The multiphonon processes analyzed in our case lead to similar effects.

Our analysis so far focused on the fundamental breathing mode which has the longest lifetime (see Table I). However, for short enough times, just after the elastic excitation, more eigenmodes are active. Moreover, due to elastic damping the variation of the optical spectrum is not periodic. In this case, the Fourier transform of $a^{+}_{Plm}(t)$ takes the form

$$a^{+}_{Plm}(t) = \int df\ \widetilde{a}^{+}_{Plm}(f)\exp(-i2\pi ft), \tag{14}$$

with

$$\widetilde{a}^{+}_{Plm}(f) = \int dt\ a^{+}_{Plm}(t)\exp(i2\pi ft), \tag{15}$$

and, similarly to Eq. (13), we define

$$\sigma_{\rm sc}(f) = \frac{1}{q^2|\mathbf{E}_0|^2}\sum_{Plm}|\widetilde{a}^{+}_{Plm}(f)|^2. \tag{16}$$

The time evolution of the scattering cross section, after launching of an initial radial linearly increasing displacement field following a homogeneous thermal excitation (see Fig. 2), is shown in the upper diagrams of Fig. 5 for the TE_7 and TM_4 Mie resonances. Attenuation is rather weak, so that the elastic vibration survives several periods. This is different compared to metallic nanoparticles with diameters of a few nanometers, reported recently.[23,26] For long enough times, only the fundamental breathing mode survives, while all other modes decay. Using a time window of 200 ns, comparable to τ_0, to evaluate the integral of Eq. (15) we obtain the ILS spectrum (bottom diagrams of Fig. 5) which exhibits three main peaks at f_0, $2f_0$, and $3f_0$ (see Table I) for the high-Q Mie resonance due to multiphonon interactions with the fundamental acoustic breathing mode, while for the low-Q Mie resonance there are only single-phonon interactions with the fundamental acoustic breathing mode. These results indicate that it is difficult to obtain a clear picture of the AO effect from the time variation of the optical cross section, while the ILS spectra justify our initial analysis of the AO interaction based on only the fundamental acoustic breathing mode. It should also be noted that, even if there are deviations from an initial homogeneous thermal excitation, the analysis based on only the fundamental acoustic breathing mode is still approximately valid, as long as this mode provides the major contribution in the expansion of the initial displacement field.

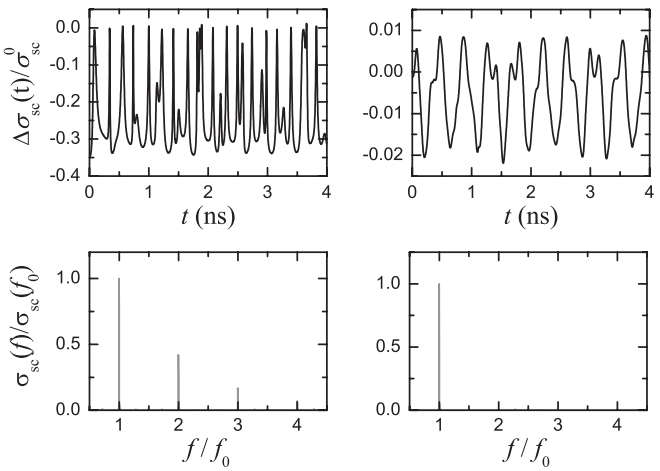

FIG. 5. Optical scattering cross section of the particle under consideration for the TE_7 (left) and TM_4 (right) Mie resonances acousticaly activated by an initial radial, linearly increasing displacement field at a level corresponding to $u_0 = 0.1$ nm (see Fig. 2). Time variation of the perturbed scattering cross section (upper diagrams) and ILS spectrum (lower diagrams).

V. CONCLUSIONS

In summary, we provided evidence for strong nonlinear AO effects in dielectric particles that support, simultaneously, acoustic and optical localized resonant modes. These effects, which can lead to efficient, enhanced modulation of light with sound through multiphonon exchange mechanisms, have been demonstrated on a specific example of a spherical particle made of a-As_2S_3. We described the excitation of acoustic breathing modes following ultrafast heating of the particle by an incident laser beam and analyzed the differences in the AO interaction between high-Q and low-Q optical resonances providing a consistent interpretation of the underlying physics. The fact that the acoustic wave is triggered by an incident light wave allows for an all-optical modulation of light mediated by phonons. It is important to note that the effects discussed here are not restricted to the specific particle size and shape, to the extent that it exhibits high-Q Mie resonances, or to the assumption of a homogeneous thermal excitation. The mechanism is expected to be more efficient at optical and near-infrared frequencies using micrometric particles of a high-refractive-index material that support low-order, high-Q Mie resonances, and have large AO coefficients.

ACKNOWLEDGMENTS

This work was supported by the European Commission Seventh Framework Programme (FP7) under the FET-Open project TAILPHOX N 233883.

*ggantzou@phys.uoa.gr

[1] V. R. Almeida, C. A. Barrios, R. R. Panepucci, and M. Lipson, Nature (London) **431**, 1081 (2004).
[2] T. Tanabe, M. Notomi, S. Mitsugi, A. Shinya, and E. Kuramochi, Appl. Phys. Lett. **87**, 151112 (2005).
[3] R. Boyd, *Nonlinear Optics*, 2nd ed. (Academic Press, London, 2003).
[4] M. Brunstein, R. Braive, R. Hostein, A. Beveratos, I. Rober-Philip, I. Sagnes, T. J. Karle, A. M. Yacomotti, J. A. Levenson, V. Moreau, G. Tessier, and Y. D. Wilde, Opt. Express **17**, 17118 (2009).
[5] M. Notomi, Rep. Prog. Phys. **73**, 096501 (2010).
[6] K. Vahala, *Optical Microcavities* (Word Scientific, Singapore, 2004).
[7] J. Leuthold, C. Koos, and W. Freude, Nat. Photon. **4**, 535 (2010).
[8] X. Hu, P. Jiang, C. Ding, H. Yang, and Q. Gong, Nat. Photon. **2**, 185 (2008).
[9] S. Weis, R. Rivière, S. Deléglise, E. Gavartin, O. Arcizet, A. Schliesser, and T. J. Kippenberg, Science **330**, 1520 (2010).
[10] O. B. Wright, Phys. Rev. B **49**, 9985 (1994).
[11] I. Favero and K. Karrai, Nat. Photon. **3**, 201 (2007).
[12] T. Berstermann, C. Brüggemann, M. Bombeck, A. V. Akimov, D. R. Yakovlev, C. Kruse, D. Hommel, and M. Bayer, Phys. Rev. B **81**, 085316 (2010).
[13] A. Huynh, N. D. Lanzillotti-Kimura, B. Jusserand, B. Perrin, A. Fainstein, M. F. Pascual-Winter, E. Peronne, and A. Lemaître, Phys. Rev. Lett. **97**, 115502 (2006).
[14] N. D. Lanzillotti-Kimura, A. Fainstein, C. A. Balseiro, and B. Jusserand, Phys. Rev. B **75**, 024301 (2007).
[15] M. Eichenfield, J. Chan, A. H. Safavi-Naeini, K. J. Vahala, and O. Painter, Opt. Express **17**, 20078 (2009).
[16] N. D. Lanzillotti-Kimura, A. Fainstein, A. Huynh, B. Perrin, B. Jusserand, A. Miard, and A. Lemaître, Phys. Rev. Lett. **99**, 217405 (2007).
[17] P. Lacharmoise, A. Fainstein, B. Jusserand, and V. Thierry-Mieg, Appl. Phys. Lett. **84**, 3274 (2004).
[18] I. E. Psarobas, N. Papanikolaou, N. Stefanou, B. Djafari-Rouhani, B. Bonello, and V. Laude, Phys. Rev. B **82**, 174303 (2010).
[19] M. Tomes and T. Carmon, Phys. Rev. Lett. **102**, 113601 (2009).
[20] I. S. Grudinin, A. B. Matsko, and L. Maleki, Phys. Rev. Lett. **102**, 043902 (2009).
[21] M. Eichenfield, J. Chan, R. M. Camacho, K. J. Vahala, and O. Painter, Nature (London) **462**, 78 (2009).
[22] A. H. Safavi-Naeini, T. P. M. Alegre, M. Winger, and O. Painter, Appl. Phys. Lett. **97**, 181106 (2010).
[23] V. Juvé, A. Crut, P. Maioli, M. Pellarin, M. Broyer, N. Del Fatti, and F. Vallée, Nano Lett. **10**, 1853 (2010).
[24] Y. Guillet, C. Rossignol, B. Audoin, G. Calbris, and S. Ravaine, Appl. Phys. Lett. **95**, 061909 (2009).
[25] Y.-S. Chen, W. Frey, S. Kim, P. Kruizinga, K. Homan, and S. Emelianov, Nano Lett. **11**, 348 (2011).
[26] D. Mongin, V. Juvé, P. Maioli, A. Crut, N. Del Fatti, F. Vallée, A. Sánchez-Iglesias, I. Pastoriza-Santos, and L. M. Liz-Marzán, Nano Lett. **11**, 3016 (2011).
[27] W. Y. Huang, W. Qian, and M. A. El-Sayed, Adv. Mater. **20**, 733 (2008).
[28] A. V. Akimov, Y. Tanaka, A. B. Pevtsov, S. F. Kaplan, V. G. Golubev, S. Tamura, D. R. Yakovlev, and M. Bayer, Phys. Rev. Lett. **101**, 033902 (2008).
[29] T. Carmon and K. J. Vahala, Phys. Rev. Lett. **98**, 123901 (2007).
[30] D. H. Broaddus, M. A. Foster, I. H. Agha, J. T. Robinson, M. Lipson, and A. L. Gaeta, Opt. Express **17**, 5998 (2009).
[31] E. D. Palik, *Handbook of Optical Constants*, 2nd ed. (Academic Press, London, 1998).
[32] G. B. Arfken, H. J. Weber, and F. Harris, *Mathematical Methods for Physicists*, 5th ed. (Academic Press, London, 2000).
[33] P. Emery and A. Devos, Appl. Phys. Lett. **89**, 191904 (2006).
[34] A. Crut, V. Juvé, D. Mongin, P. Maioli, N. Del Fatti, and F. Vallée, Phys. Rev. B **83**, 205430 (2011).
[35] A. Yariv and P. Yeh, *Optical Waves in Crystals* (John Wiley and Sons, New Jersey, 2003).
[36] R. K. Galkiewicz and J. Tauc, Solid State Commun. **10**, 1261 (1972).
[37] J. D. Jackson, *Classical Electrodynamics*, 3rd ed. (Wiley, New York, 1998).
[38] N. Stefanou, C. Tserkezis, and G. Gantzounis, Proc. SPIE **6989**, 698910 (2008).
[39] C. Bohren and D. Huffman, *Absorption and Scattering of Light by Small Particles* (Wiley, New York, 1983).